Direct writing of room temperature polariton condensate lattice

Ravindra Kumar Yadav,*,† Sitakanta Satapathy,† Prathmesh Deshmukh,†,||
Biswajit Datta,† Addhyaya Sharma,† Andrew H. Olsson,‡ Junsheng Chen,¶ Bo
W. Laursen,¶ Amar H. Flood,‡ Matthew Y. Sfeir,§ and Vinod M. Menon*,†,||

†Department of Physics, The City College of New York, 85 St. Nicholas Terrace, 85 St. Nicholas Terrace, New York, 10031, USA.

‡Department of Chemistry, Indiana University, IN 47405, USA

¶Nano-Science Center and Department of Chemistry, University of Copenhagen, Denmark. §Photonics Initiative, Advanced Science Research Center, City University of New York, New York,

85 St. Nicholas Terrace, New York, 10031, USA.

||The PhD Program in Physics, Graduate Center of the City University of New York, 365 5th Ave,
New York, 10016, USA.

E-mail: ryadav@ccny.cuny.edu; vmenon@ccny.cuny.edu

Abstract

Realizing lattices of exciton polariton condensates has been of much interest owing to the potential of such systems to realize analog Hamiltonian simulators and physical computing architectures. Here, we report the realization of room temperature polariton condensate lattice using a direct-write approach. Polariton condensation is achieved in a microcavity embedded with host-guest Frenkel excitons of an organic dye (rhodamine) in a small molecular ionic isolation lattice

(SMILES) . The microcavity is patterned using Focused Ion Beam etching to realize arbitrary lattice geometries including defect sites on demand. The band structure of the lattice and the emergence of condensation are imaged using momentum-resolved spectroscopy. The introduction of defect sites is shown to lower the condensation threshold and result in the formation of a defect band in the condensation spectrum. The present approach allows us to study periodic, quasi-periodic, and disordered polariton condensate lattices at room temperature using a direct-write approach.

Keywords: Polariton, Molecular polaritons, Polariton condensation, Polariton lattice, Condensate lattice

Exciton-polaritons are hybrid quasiparticles that arise from the strong coupling between excitons in semiconductors and cavity photons in microcavities. These polaritons possess a small effective mass inherited from the photonic component, as well as strong interactions stemming from the excitonic part. The combination of small effective mass, interaction effects, and bosonic nature enables the observation of intriguing phenomena like Bose-Einstein-like condensation, superfluidity, and vortex formation. ¹⁻⁶ The realization of exciton-polariton condensate lattices has emerged as an attractive platform for analog Hamiltonian simulators, such as the classical XY Hamiltonian, and for physical computing architectures. 7-12 Previous studies on polariton condensate lattices have primarily focused on GaAs-based systems, ^{13–19} with recent advancements in organic molecules and perovskite systems allowing for room temperature operation. 12,20-24 However, most of these room temperature systems rely on patterning the bottom mirror before deposition of the active material due to detrimental effect of patterning the cavity after fabrication or via structured illumination. ^{20–23} This significantly limits the types of lattices and more importantly the refractive index contrast that can be achieved. Here, we present an approach where the planar microcavity after fabrication is patterned to realize arbitrary lattice geometries using a direct-write approach that utilizes Focused Ion Beam (FIB) etching. This etching technique enables the realization of high refractive index contrast lattices, similar to those demonstrated in GaAs systems. 25 Specifically, we report direct writing of a two-dimensional exciton-polariton condensate lattice by patterning an array of overlapping pillars etched into a planar microcavity. Defect sites were also introduced into the

cavity by adding or removing pillars. The patterned microcavity structure shows condensation at room temperature along with the bands arising from the lattice structure as well as the emergence of defect state condensation. To characterize the fabricated lattice, we employ energy-resolved wavevector imaging of photoluminescence (PL) and perform power-dependent PL measurements to study optical nonlinearities.

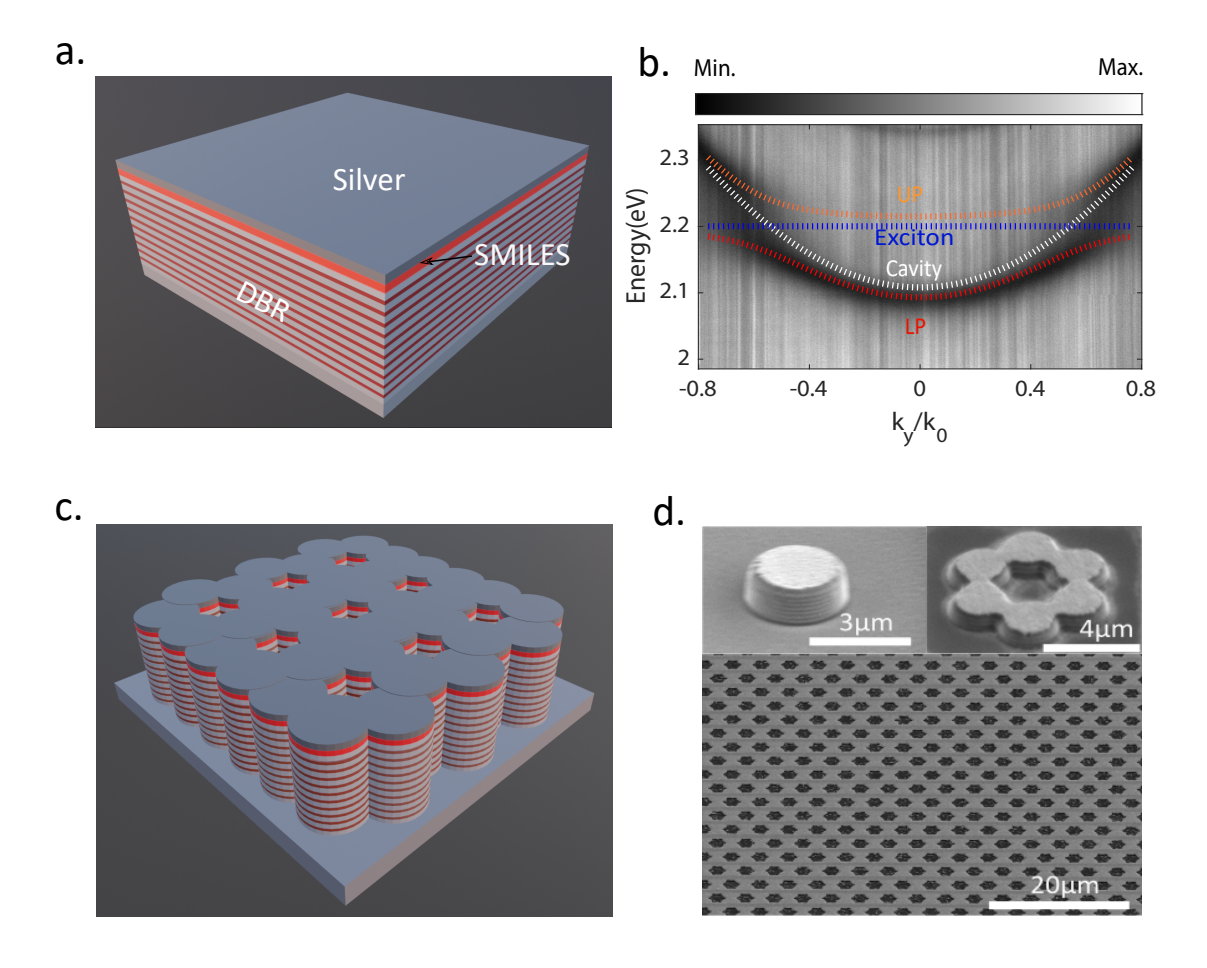


Figure 1: (a) Schematic for planar organic exciton-polariton cavity. (b) White light angle-dependent reflectivity of the planar cavity region along with coupled oscillator model fits to the observed dispersion. (c) Schematic for patterned honeycomb organic exciton-polariton lattice. (d) Scanning electron microscope image of a single micropillar, honeycomb unit cell, and lattice patterned on the planar cavity using FIB.

Here, we fabricate an exciton-polariton microcavity on a glass substrate, as shown in Fig.1 a. The cavity consists of a 10.5-pair bottom distributed Bragg reflector (DBR) consisting of alternating layers of a quarter wavelength thick SiO_2 and TiO_2 deposited via radio-frequency sputtering.

The center wavelength of the bottom DBR was designed to be around $600 \, nm$, and the bandwidth was $\sim 200 \, nm$. We use the recently introduced organic dye, small molecule ionic isolation lattice (SMILES) system as the excitonic material owing to their enhanced photostability and high quantum yield. 24,26,27 Specifically, we use rhodamine 3B (R3B), a widely used laser dye (with bandgap $\sim 2.19 \, eV$, $\sim 566 \, nm$), composed as a SMILES material (See methods)(Supporting Information(SI), Fig.S1). $\sim 30 \, nm$ R3B-SMILES in PMMA matrix is deposited via spin coating onto the bottom DBR as shown in Fig.1a. The cavity is completed by depositing $\sim 100 \, nm$ thick silver film on top of the SMILES layer. This results in the formation of a Tamm plasmon cavity mode with loaded Q of $\sim 200 \, \text{similar}$ to our previous report. 24 Strong coupling between the Tamm mode and the excitons of the SMILES results in the formation of polariton states whose dispersion obtained via Fourier imaging is shown in Fig.1b along with fits based on the coupled oscillator model. Anticrossing between the upper(UP) and lower polariton(LP) branches is observed at finite in-plane momentum due to the negative detuning ($40 \, meV$) of the cavity with respect to the exciton in SMILES. The estimated Rabi splitting based on the coupled oscillator model fit is $100 \, meV$.

The strongly coupled cavity is patterned using FIB etching with low ion current $(77 \ pA)$ and $30 \ kV$ voltage to avoid heating caused by the gallium ion beam. The microcavity is patterned into different structures, such as a single pillar, honeycomb unit cell, and honeycomb lattice, as shown schematically in Fig. 1c. The scanning electron microscope images of the patterned structures are shown in Fig. 1d.

In the single pillar case, the refractive index contrast arising from the etching of the pillar (diameter= $2.75 \ \mu m$) results in lateral confinement and emergence of discrete polariton states²⁸ as opposed to dispersive branches observed in planar cavities as shown in SI, Fig.S2a. When the excitation power is increased above the condensation threshold ($1.25 \ p_{th}$) the emission is observed from the lowest energy state as seen in SI, Fig.S2b.The emission linewidth below threshold was found to be the same ($\sim 7 \ nm$) before and after etching.²⁴ The smallest pillar diameter was limited by the resolution of the FIB etching approach and was found to be $\sim 2 \ \mu m$.

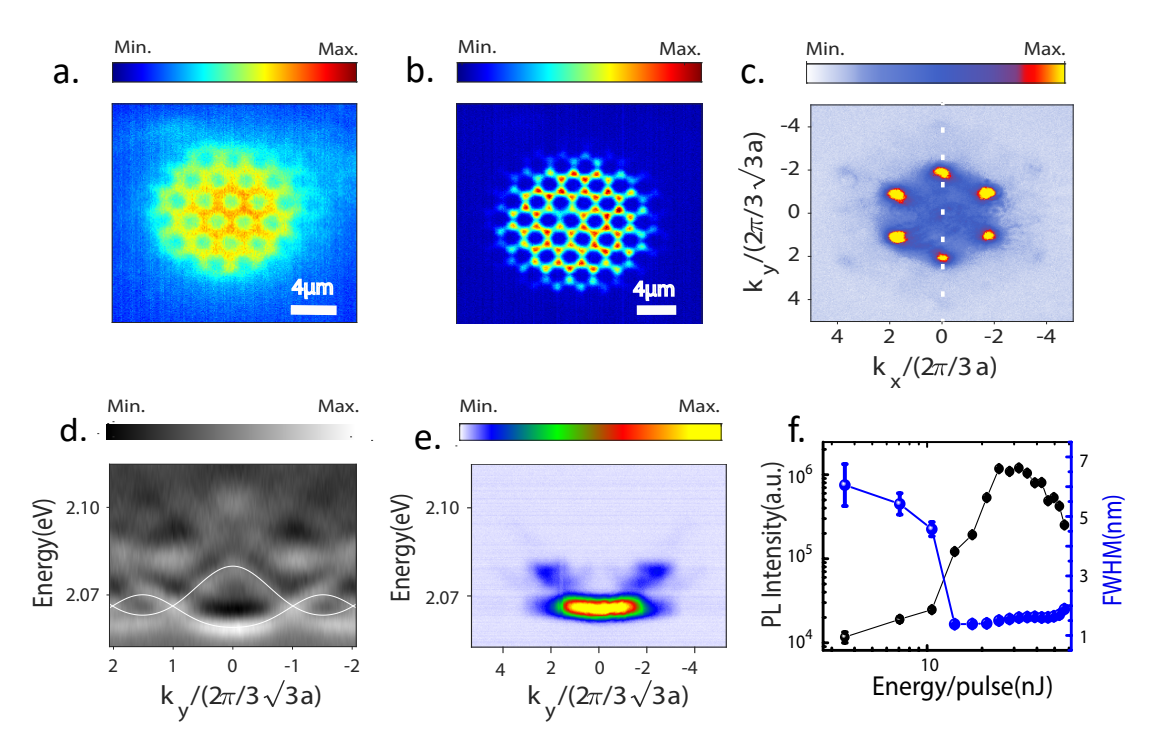


Figure 2: Measured real space PL image of honeycomb lattice (a) below condensation threshold and (b) above condensation threshold. (c) Measured momentum space PL emission image of condensate lattice above condensation threshold showing the condensation at the corners of the BZ. Energy resolved momentum space PL along the line $k_x = 0$ (white dotted in (c)) (d) below condensation threshold along with tight binding model fits to the observed dispersion and (e) above condensation threshold. (f) Integrated PL intensity and full width at half maximum (FWHM) of condensate lattice PL as a function of pulse energy.

Two-dimensional array of micropillars in a honeycomb lattice geometry with micropillar diameter (d) 2.75 μ m and lattice constant (a) 2.40 μ m is realized using FIB etching following similar approach to the single pillar. The polariton lattice is excited non-resonantly at 514 nm wavelength using a flat top beam with a spot size of approximately 25 μ m, generated by tightly focusing 280 femtosecond(fs) pulsed laser with a repetition rate of 1 KHz on the back focal plane of a 50x microscope objective (numerical aperture=0.80) (See Methods for more details). Fig.2a and 2b illustrate the real-space PL of the lattice below and above the condensation threshold (pulse energy=10 nJ), respectively. A distinct transition is observed from delocalized PL to localized PL, specifically at the lattice sites. Fig.2c displays the momentum resolved image of the PL from the lattice after condensation, demonstrating the localization of polariton PL at the six Dirac points of the first

Brillouin Zone(BZ). Fig.2d shows the experimentally observed band structure of the honeycomb lattice in energy resolved momentum space PL with the momentum slice taken along k_x =0 (dashed line in Fig.2c) below the condensation threshold. Modified bandstructure along other in-plane momentum directions are shown in SI Fig.S3a-c. Above the threshold, we observe the collapse of PL to the lowest energy bands as shown in Fig.2e. Pump power dependence of emission intensity and linewidth is shown in Fig.2f. Clear threshold and nonlinear increase in output intensity is observed along with the decrease in the linewidth indicative of the onset of polariton condensation similar to what was reported previously in non-patterned SMILES system.²⁴

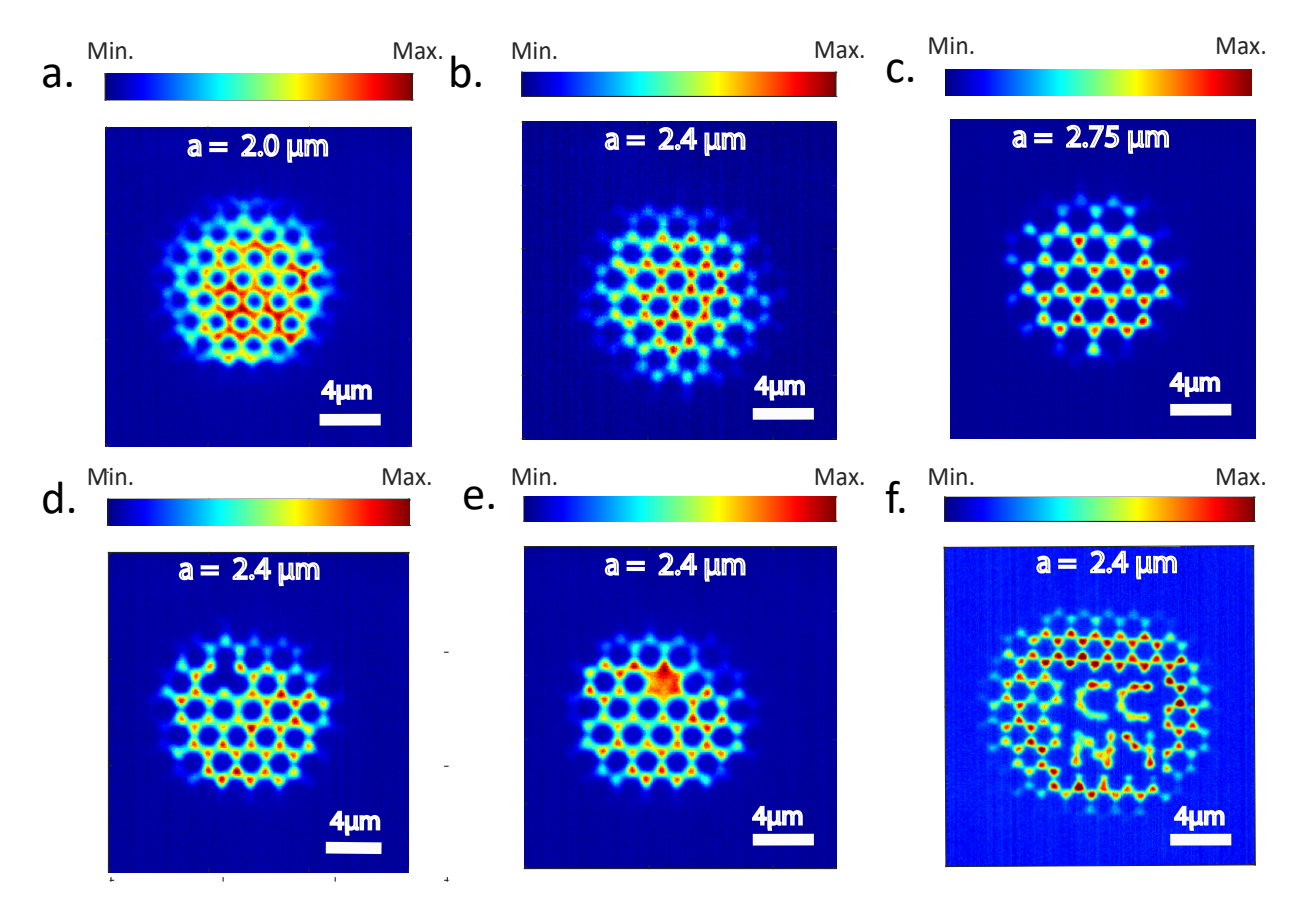


Figure 3: Real space PL image of polariton condensate lattice with micropillar diameter d=2.75 μm , and lattice constant (a) a = 2.0 μm , (b) a = 2.4 μm , (c) a = 2.75 μm ,(d) a = 2.4 μm with missing lattice sites defect,(e) a = 2.4 μm with missing hole, (f) a = 2.4 μm with "CCNY" logo as an example of arbitrary defects that can be realized through design.

Finally, we investigate polariton condensation in 2D honeycomb lattices with varying degree of coupling between the lattice sites and on the presence of defects. Fig.3a-c, show the real space

image of condensation in lattices with varying degree of coupling between lattice sites with lattice constant varying from $a = 2.0 \,\mu m$ to 2.75 μm . We observe the transition from delocalized to localized condensate formation by increasing the inter-pillar distance (reduced intersite coupling). For the highly coupled case (Fig.3a), the condensate is delocalized over the entire structure in contrast to the weakly coupled case (Fig.3c), where the condensates are localized at the pillar sites. Nevertheless, owing to the evanescent coupling between the lattice sites, we expect spatial coherence across the entire pump spot as was previously shown. ²⁴ The versatility of our direct-write approach is shown in Fig.3 d-f, where lattices with a missing pillar (Fig.3d), missing hole (Fig.3e) and arbitrary defect pattern showing the abbreviation of City College of New York (CCNY) (Fig.3f) are realized. We also studied the role of lattice defects in the condensate formation. Shown in Fig.4 a-c is the real space image of the PL from the lattice for increasing pump power. Below the condensation threshold, the PL is distributed throughout the lattice. The onset of condensation is observed first at the defect site (Fig.4b), followed eventually by condensation emerging across the entire lattice. The threshold for condensation at the lattice site $(p_{th} \sim 7 \ nJ)$ is lower than what was observed previously in defect-free lattices ($p_{th} \sim 10 \ nJ$), indicating enhanced scattering to the defect site as shown in Fig.4d. To observe the defect energy state, we realized structures with increased density of defects by creating array of missing hole defect in lattice. Shown in Fig.4e is the real space PL of the array of missing hole defects above condensation threshold. Defect energy state is observed in the momentum resolved emission at lower energy state as shown in Fig.4f. We also realized structures with random distribution of defects where, once again condensation was found to occur at the defect sites and the band structure showed lower energy defect band (SI,Fig.S4).

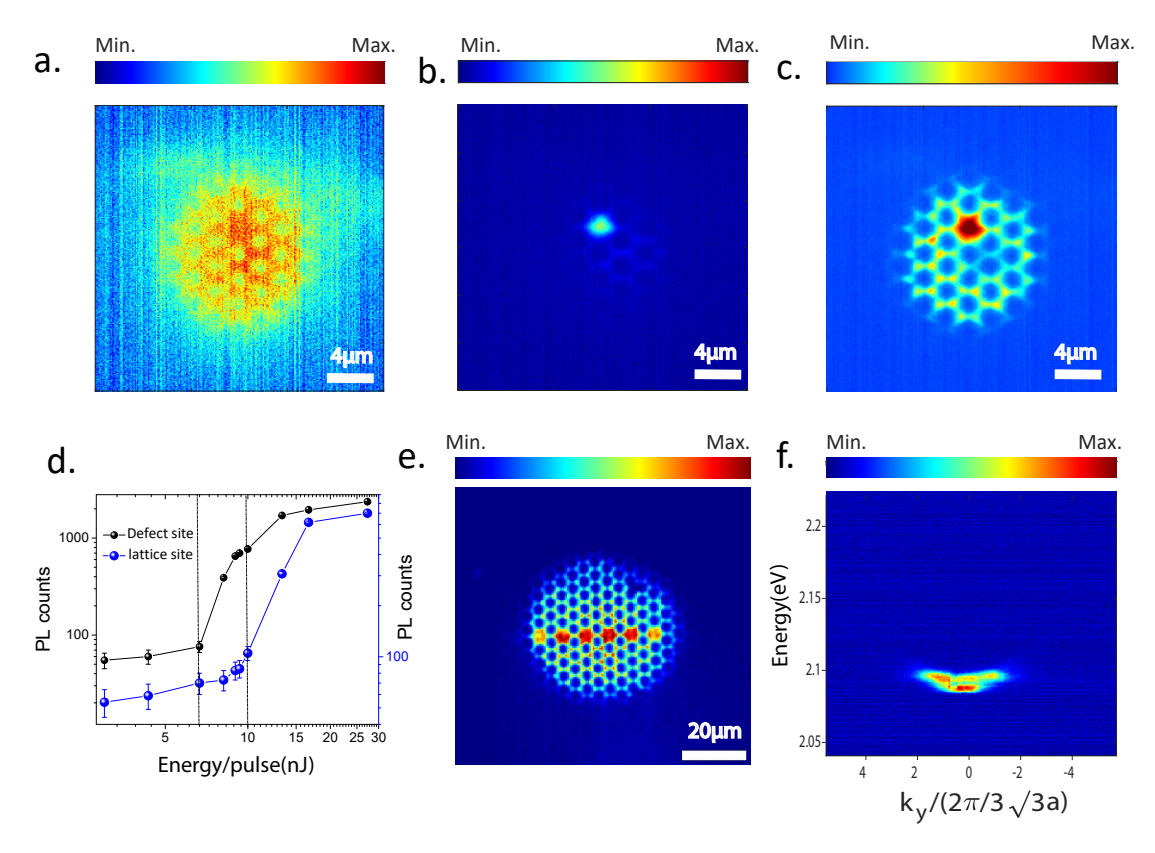


Figure 4: Real space PL image of defect lattice with missing hole at input power, (a) $p = 0.5p_{th}$ collected for longer integration time (30 sec) to show background lattice below condensation threshold on defect site of lattice, (b) $p = p_{th}$ collected with integration time 1 sec and (c) $p = 1.25p_{th}$ collected with integration time 1 sec. Preferential condensation at the lattice defect site is observed. (d) Condensate lattice PL counts at defect sites and lattice cite as a function of pulse energy. The vertical dotted lines show threshold energies of $p_{th} \sim 7 \, nJ$ and $\sim 10 \, nJ$ for the defect site and the defect free lattice, respectively. (e) Real space PL image of defect lattice array with missing holes at $p = 1.25p_{th}$, (f) Energy resolved momentum space PL showing lower energy emission band arising from the defect states at $p = 1.25p_{th}$.

.

In summary, we report the realization of room temperature polariton condensate lattice using a direct-write fabrication approach involving FIB etching on the host-guest-based organic SMILES microcavity. Experimental results demonstrate the confinement of polaritons resulting in discrete states and condensation to the ground state energy in the single micropillars. Through the patterning of a honeycomb lattice, we realized polariton condensate lattice consisting of coupled micropillars. By changing the lattice constant, we demonstrate the transition from delocalized to localized condensate. Furthermore, we study the effect of deterministically placed defects in the

condensate lattice, revealing that condensates prefer high refractive index sites for localization and also reduce the condensation threshold pump power. The SMILES microcavity facilitates direct-write approach, thus providing a versatile and scalable platform for studying arbitrary polariton condensate lattices and polaritonic circuits at room temperature over large area. While the present demonstration was carried out with silver top mirror, the use of dielectric mirrors deposited via sputtering or mechanical transfer will enhance the quality factor of the cavity and help in reducing the threshold as well the linewdith.

Methods

SMILES microcavity fabrication

To prepare the SMILES solution, we followed a previously reported recipe. 24,26 The SMILES-based microcavity is fabricated on a quartz substrate with distributed Bragg reflector (DBR) centered at 620 nm. The DBR, composed of 10.5 pairs of SiO_2/TiO_2 , was cleaned using O_2 plasma for 5 minutes. A ~ 30 nm thick SMILES film is then deposited on the cleaned DBR using a spin coating technique with a two-step process. In the first step, the film is spun for 20 seconds at a speed of 1000 rpm, followed by a second step of spinning for 80 seconds at 3000 rpm. The deposited SMILES film is placed in a constant pressure vacuum at 25 °C. Finally, a ~100 nm thick silver layer is deposited on top of the SMILES film using an e-beam evaporator, completing the fabrication of the microcavity.

Experimental techniques

We employed real space PL and Fourier space PL imaging to map the condensate emission characteristics and the band structure of the lattice. For our measurements, we utilized two lasers. To investigate the band structures, we used a 488 *nm* laser (NKT SuperK) with a repetition rate of 76 *MHz* to excite the patterned structure on the silver sides of the microcavity. For the excitation

of the larger area in the lattice, we created a large laser spot ($\sim 25~\mu m$) by focusing the laser on the back focal plane of the objective lens. The band structure of the lattice is measured using far-field imaging techniques, where the back focal plane of the objective lens is imaged in front of a charged coupled device(CCD) camera (PIXIS 1024). Energy-resolved angle-dependent PL was measured by selecting a specific in-plane momentum using a monochromator (Princeton Instruments) in front of the CCD camera and dispersing the PL using a 300 grooves per line grating. We employed a pulsed 514 nm laser (Carbide from Light Conversion) with a pulse width of 280 fs and a repetition rate of 1 kHz for the condensation experiments. The Brillouin zone and band structure were measured using the Fourier imaging technique.

Coupled oscillator model

Upper and lower polariton branches in reflectivity of the strongly coupled cavity are fit using coupled oscillator model defined by following Hamiltonian:

$$H = \begin{bmatrix} E_x(k) - \iota \gamma_x / 2 & g \\ g & E_c(k) - \iota \gamma_c / 2 \end{bmatrix}$$
 (1)

Where g is the coupling strength between exciton and single cavity mode. $E_x(k)$ and $E_c(k)$ are the energy of exciton and cavity mode, respectively. γ_x and γ_c are full width at half maximum(FWHM) of exciton and cavity mode resonance, respectively.

Tight binding model for bandstructure

Tight binding approximation is used to fit the bandstructure of the honeycomb polariton lattice. The tight binding model for honeycomb polariton lattice is given by the following expression: ²⁵

$$E(k) = \pm t_n \sqrt{3 + F(k)} - t_{nn} F(k)$$
 (2)

where F(k) is expressed as:

$$F(k) = 2\cos\sqrt{3}k_{y}a + 4\cos\frac{\sqrt{3}}{2}k_{y}a.\cos\frac{3}{2}k_{x}a$$
 (3)

where t_n and t_{nn} are coupling to the first and second nearest neighbor and used as free parameters in the fitting. Extracted value of t_{nn}/t_n is ~ 0.10, which is in good agreement with the previously reported pattern structure through etching.²⁵

Supporting Information

Absorption and photoluminescence of SMILES, Polariton condensation in single micropillar, Bandstructure of honeycomb polariton lattice, Effect of random missing hole defects in polariton lattice condensate.

Acknowledgments

V.M.M. and R.K.Y. were supported by the U.S. Air Force Office of Scientific Research–MURI Grant FA9550–22–1–0317. S.S., and P.D., acknowledge support from the US National Science Foundation (OMA–1936351). B.D. and A.S. were supported by the Army Research Office Grant W911NF–22–1–0091. M.Y.S. work was supported by the U.S. Department of Energy, Office of Science, Office of Basic Energy Sciences under Award No. DE–SC0022036. A.H.O. and A.H.F. acknowledge support from the U.S. National Science Foundation (DMR–2118423).

Declarations

Financial Declaration: The authors declare the following competing financial interest(s): A.H.F. and B.W.L. are cofounders in Halophore, Inc. R.K.Y., S.S., P.D., V.M.M., B.W.L., and A.H.F. have filed a provisional patent application.

Data Availability

All data will be provided by the corresponding authors upon reasonable request.

References

- (1) Deng, H.; Haug, H.; Yamamoto, Y. Exciton-polariton bose-einstein condensation. *Reviews of modern physics* **2010**, 82, 1489.
- (2) Byrnes, T.; Kim, N. Y.; Yamamoto, Y. Exciton–polariton condensates. *Nature Physics* **2014**, *10*, 803–813.
- (3) Keeling, J.; Kéna-Cohen, S. Bose–Einstein condensation of exciton-polaritons in organic microcavities. *Annual Review of Physical Chemistry* **2020**, *71*, 435–459.
- (4) Amo, A.; Lefrère, J.; Pigeon, S.; Adrados, C.; Ciuti, C.; Carusotto, I.; Houdré, R.; Giacobino, E.; Bramati, A. Superfluidity of polaritons in semiconductor microcavities. *Nature Physics* 2009, 5, 805–810.
- (5) Lagoudakis, K. G.; Wouters, M.; Richard, M.; Baas, A.; Carusotto, I.; André, R.; Dang, L. S.; Deveaud-Plédran, B. Quantized vortices in an exciton–polariton condensate. *Nature physics* 2008, 4, 706–710.
- (6) Nardin, G.; Grosso, G.; Léger, Y.; Pitka, B.; Morier-Genoud, F.; Deveaud-Plédran, B. Hy-

- drodynamic nucleation of quantized vortex pairs in a polariton quantum fluid. *Nature Physics* **2011**, *7*, 635–641.
- (7) Berloff, N. G.; Silva, M.; Kalinin, K.; Askitopoulos, A.; Töpfer, J. D.; Cilibrizzi, P.; Langbein, W.; Lagoudakis, P. G. Realizing the classical XY Hamiltonian in polariton simulators. *Nature materials* **2017**, *16*, 1120–1126.
- (8) Amo, A.; Bloch, J. Exciton-polaritons in lattices: A non-linear photonic simulator. *Comptes Rendus Physique* **2016**, *17*, 934–945.
- (9) Kavokin, A.; Liew, T. C.; Schneider, C.; Lagoudakis, P. G.; Klembt, S.; Hoefling, S. Polariton condensates for classical and quantum computing. *Nature Reviews Physics* **2022**, *4*, 435–451.
- (10) Ballarini, D.; Gianfrate, A.; Panico, R.; Opala, A.; Ghosh, S.; Dominici, L.; Ardizzone, V.; De Giorgi, M.; Lerario, G.; Gigli, G.; others Polaritonic neuromorphic computing outperforms linear classifiers. *Nano Letters* 2020, 20, 3506–3512.
- (11) Mirek, R.; Opala, A.; Comaron, P.; Furman, M.; Król, M.; Tyszka, K.; Seredynski, B.; Ballarini, D.; Sanvitto, D.; Liew, T. C.; others Neuromorphic binarized polariton networks. *Nano letters* **2021**, *21*, 3715–3720.
- (12) Tao, R.; Peng, K.; Haeberlé, L.; Li, Q.; Jin, D.; Fleming, G. R.; Kéna-Cohen, S.; Zhang, X.; Bao, W. Halide perovskites enable polaritonic XY spin Hamiltonian at room temperature.
 Nature Materials 2022, 21, 761–766.
- (13) Kéna-Cohen, S.; Forrest, S. Room-temperature polariton lasing in an organic single-crystal microcavity. *Nature Photonics* **2010**, *4*, 371–375.
- (14) Daskalakis, K.; Maier, S.; Murray, R.; Kéna-Cohen, S. Nonlinear interactions in an organic polariton condensate. *Nature materials* **2014**, *13*, 271–278.

- (15) Plumhof, J. D.; Stöferle, T.; Mai, L.; Scherf, U.; Mahrt, R. F. Room-temperature Bose–Einstein condensation of cavity exciton–polaritons in a polymer. *Nature materials* **2014**, *13*, 247–252.
- (16) Grant, R. T.; Michetti, P.; Musser, A. J.; Gregoire, P.; Virgili, T.; Vella, E.; Cavazzini, M.; Georgiou, K.; Galeotti, F.; Clark, C.; others Efficient radiative pumping of polaritons in a strongly coupled microcavity by a fluorescent molecular dye. *Advanced Optical Materials* 2016, 4, 1615–1623.
- (17) Cookson, T.; Georgiou, K.; Zasedatelev, A.; Grant, R. T.; Virgili, T.; Cavazzini, M.; Galeotti, F.; Clark, C.; Berloff, N. G.; Lidzey, D. G.; others A yellow polariton condensate in a dye filled microcavity. *Advanced Optical Materials* **2017**, *5*, 1700203.
- (18) Wei, M.; Rajendran, S. K.; Ohadi, H.; Tropf, L.; Gather, M. C.; Turnbull, G. A.; Samuel, I. D. Low-threshold polariton lasing in a highly disordered conjugated polymer. *Optica* **2019**, *6*, 1124–1129.
- (19) Su, R.; Fieramosca, A.; Zhang, Q.; Nguyen, H. S.; Deleporte, E.; Chen, Z.; Sanvitto, D.; Liew, T. C.; Xiong, Q. Perovskite semiconductors for room-temperature exciton-polaritonics. *Nature Materials* 2021, 20, 1315–1324.
- (20) Dusel, M.; Betzold, S.; Egorov, O. A.; Klembt, S.; Ohmer, J.; Fischer, U.; Höfling, S.; Schneider, C. Room temperature organic exciton–polariton condensate in a lattice. *Nature communications* **2020**, *11*, 2863.
- (21) Scafirimuto, F.; Urbonas, D.; Becker, M. A.; Scherf, U.; Mahrt, R. F.; Stöferle, T. Tunable exciton–polariton condensation in a two-dimensional Lieb lattice at room temperature. *Communications Physics* **2021**, *4*, 39.
- (22) Jayaprakash, R.; Whittaker, C. E.; Georgiou, K.; Game, O. S.; McGhee, K. E.; Coles, D. M.; Lidzey, D. G. Two-dimensional organic-exciton polariton lattice fabricated using laser patterning. *ACS Photonics* **2020**, *7*, 2273–2281.

- (23) Su, R.; Ghosh, S.; Wang, J.; Liu, S.; Diederichs, C.; Liew, T. C.; Xiong, Q. Observation of exciton polariton condensation in a perovskite lattice at room temperature. *Nature Physics* **2020**, *16*, 301–306.
- (24) Deshmukh, P.; Satapathy, S.; Michail, E.; Olsson, A. H.; Bushati, R.; Yadav, R. K.; Khatoniar, M.; Chen, J.; John, G.; Laursen, B. W.; others Plug-and-Play Molecular Approach for Room Temperature Polariton Condensation. *ACS Photonics* **2024**, *11*, 348–355.
- (25) Jacqmin, T.; Carusotto, I.; Sagnes, I.; Abbarchi, M.; Solnyshkov, D.; Malpuech, G.; Galopin, E.; Lemaître, A.; Bloch, J.; Amo, A. Direct observation of Dirac cones and a flatband in a honeycomb lattice for polaritons. *Physical review letters* **2014**, *112*, 116402.
- (26) Benson, C. R.; Kacenauskaite, L.; VanDenburgh, K. L.; Zhao, W.; Qiao, B.; Sadhukhan, T.; Pink, M.; Chen, J.; Borgi, S.; Chen, C.-H.; others Plug-and-play optical materials from fluorescent dyes and macrocycles. *Chem* 2020, 6, 1978–1997.
- (27) Kacenauskaite, L.; Stenspil, S. G.; Olsson, A. H.; Flood, A. H.; Laursen, B. W. Universal Concept for Bright, Organic, Solid-State Emitters Doping of Small-Molecule Ionic Isolation Lattices with FRET Acceptors. *Journal of the American Chemical Society* 2022, 144, 19981– 19989.
- (28) Galbiati, M.; Ferrier, L.; Solnyshkov, D. D.; Tanese, D.; Wertz, E.; Amo, A.; Abbarchi, M.; Senellart, P.; Sagnes, I.; Lemaître, A.; others Polariton condensation in photonic molecules. *Physical review letters* **2012**, *108*, 126403.

Direct writing of room temperature polariton condensate lattice

Ravindra Kumar Yadav,*,† Sitakanta Satapathy,† Prathmesh Deshmukh,†,||
Biswajit Datta,† Addhyaya Sharma,† Andrew H. Olsson,‡ Junsheng Chen,¶ Bo
W. Laursen,¶ Amar H. Flood,‡ Matthew Y. Sfeir,§ and Vinod M. Menon*,†,||

†Department of Physics, The City College of New York, 85 St. Nicholas Terrace, 85 St. Nicholas Terrace, New York, 10031, USA.

‡Department of Chemistry, Indiana University, IN 47405, USA

¶Nano-Science Center and Department of Chemistry, University of Copenhagen, Denmark.

§Photonics Initiative, Advanced Science Research Center, City University of New York, New York, 85 St. Nicholas Terrace, New York, 10031, USA.

||The PhD Program in Physics, Graduate Center of the City University of New York, 365 5th Ave,
New York, 10016, USA.

E-mail: ryadav@ccny.cuny.edu; vmenon@ccny.cuny.edu

Absorption and photoluminescence of SMILES

Fig.S1 shows absorption and photoluminescence of thin SMILES film on glass. Absorption spectra are measured using a UV-Vis spectrometer, and the PL of the thin film was collected by exciting SMILEs material using a 514 *nm* laser.

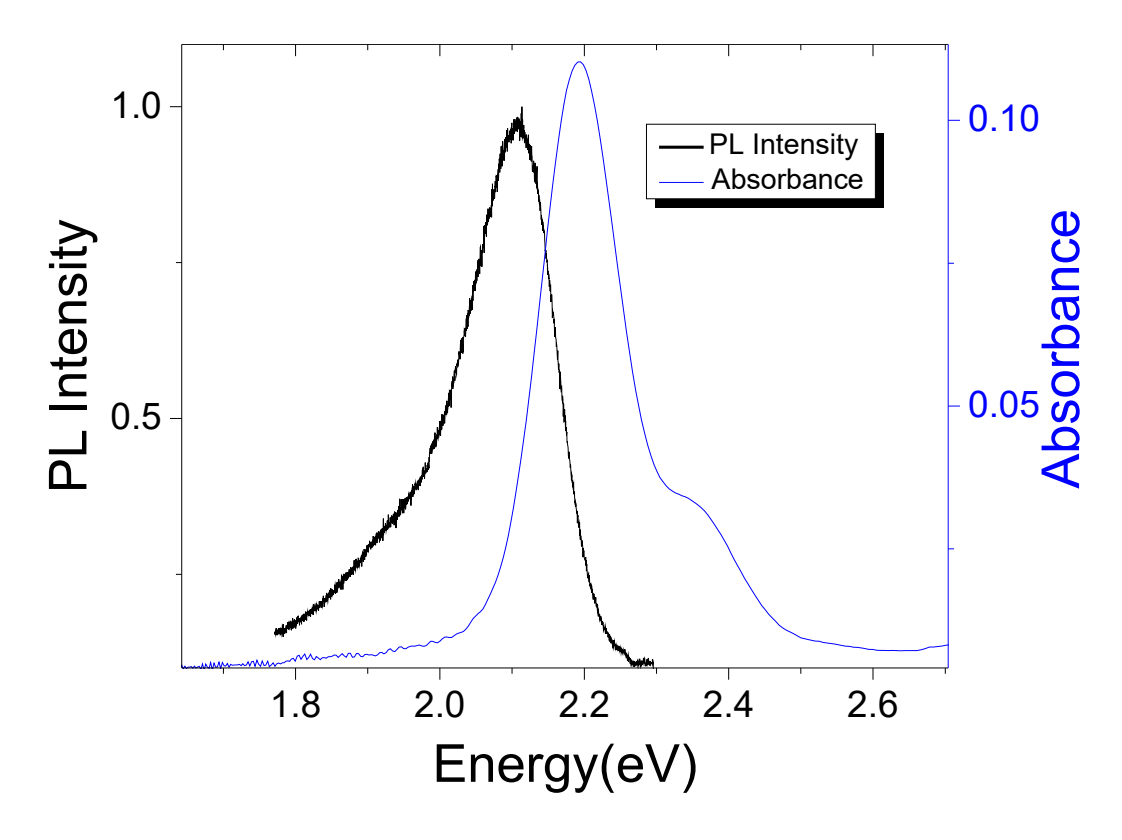


Fig. S1: Absorbance and normalized PL intensity of SMILES film on glass

Polarition condensation in single micropillar

We demonstrate the polariton condensation in a single micropillar using energy-resolved momentum space PL. Fig.S2a and b show a single micropillar's energy-resolved momentum space PL below and above the condensation threshold.

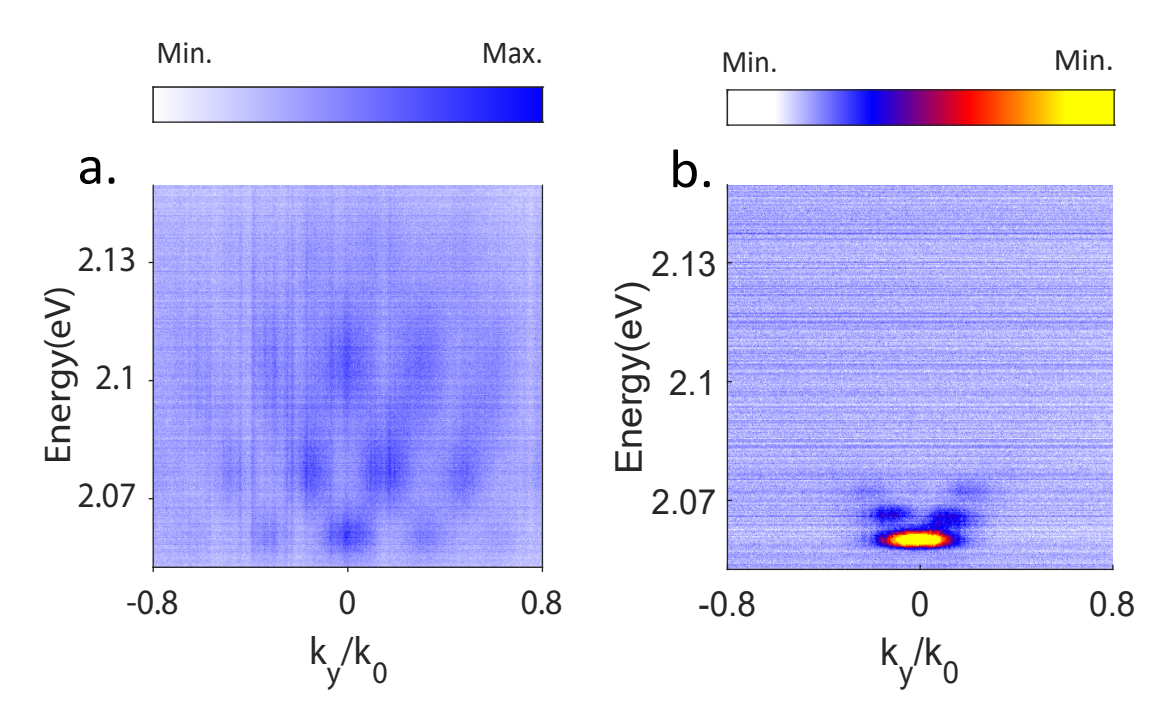


Fig. S2: Momentum space energy resolved PL from micropillar with diameter, $d = 2.75 \, \mu \text{m}$ under (a) linear regime at $p < p_{th}$ and non-linear regime at (b) $p = 1.25 \, p_{th}$

Bandstructure of honeycomb polariton lattice

PL from the honeycomb lattice is captured using energy-resolved momentum space imaging, employing a non-resonant pulsed laser (514nm) with a repetition rate of 76 MHz and a spot size of 25 μm . In the low excitation limit, the incoherent relaxation of polaritons leads to the population of all energy bands. The first Brillouin zone (BZ) of the lattice is measured using Fourier imaging at Dirac energy, as depicted in Fig.S3a. Dirac points are observed as bright spots at the six corners of the measured first BZ. Energy bands of the honeycomb polariton lattice are measured along line 1 and line 2 (black lines in Fig.S3a). Fig.S3b displays the energy bands along line 1, exhibiting Dirac points at $k_x/k_0 = 0, \pm (2\pi/3a)$, accompanied by other higher-order energy bands. The measured bandstructure along line 2, away from the Dirac point, displays energy bands with a resolved energy gap, as illustrated in Fig.S3c.

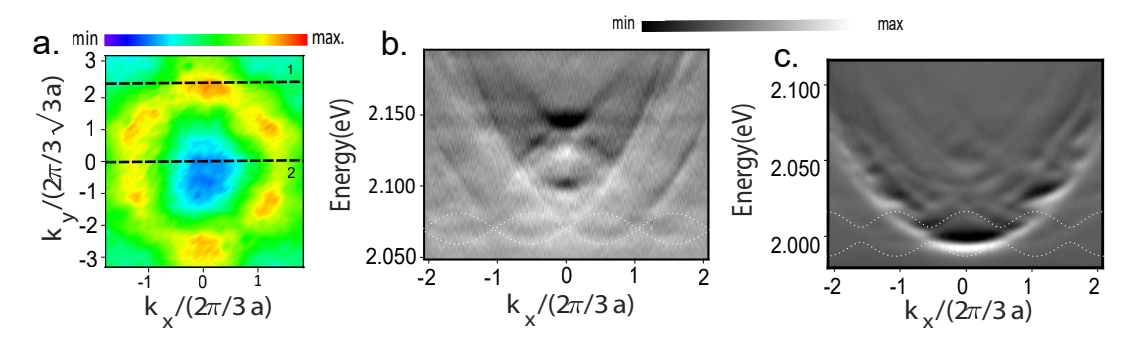


Fig. S3: (a) Measured BZ of the honeycomb lattice at the Dirac energy. Experimentally measured band structure along with tight binding model fits to the observed dispersion along (b) line 1 at $k_y = 4\pi/(3\sqrt{3}a)$ and (c) line 2 at $k_y = 0$ in (a).

Effect of random defects in polariton lattice condensate

We also studied the effect of larger density of missing hole defects in honeycomb lattice on polariton condensates. The results are shown in Fig.S4. Similar results are observed as presented in the main manuscript in case of missing hole defect array in the lattice.

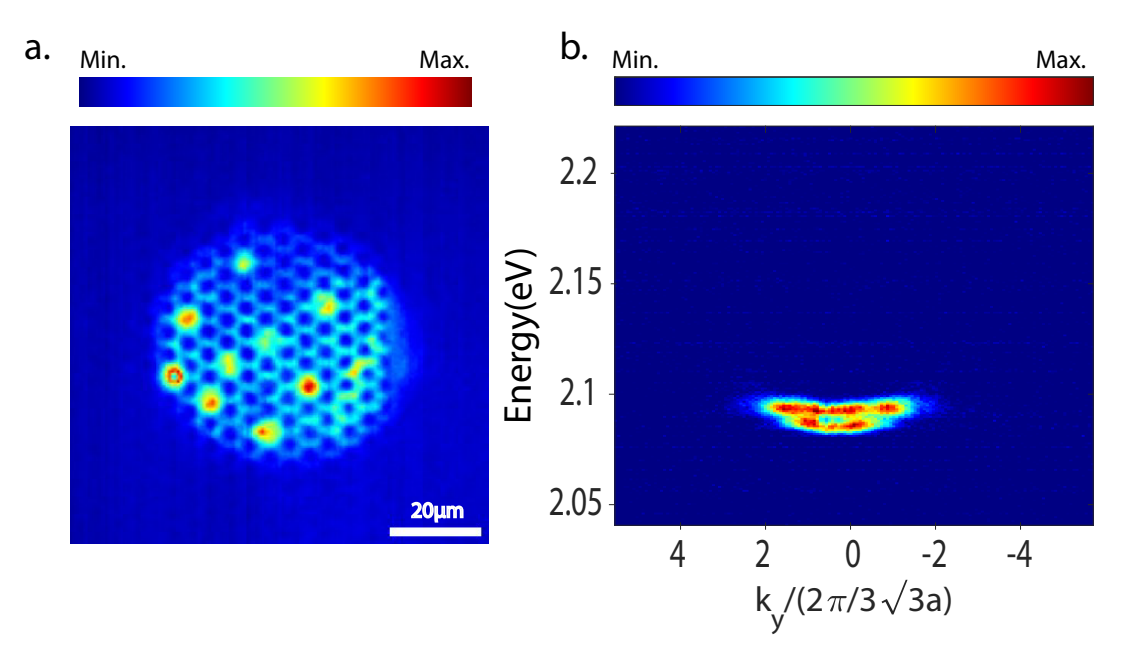


Fig. S4: (a) Real space PL image of random defects with missing holes at $p = 1.25p_{th}$, (b) Energy resolved momentum space PL showing lower energy emission band arising from the defect states at $p = 1.25p_{th}$.